Tetraploid cells from cytokinesis failure induce aneuploidy and spontaneous transformation of mouse ovarian surface epithelial cells

Cell Cycle 11:15, 2864-2875; August 1, 2012; © 2012 Landes Bioscience

Tetraploid cells from cytokinesis failure induce aneuploidy and spontaneous transformation of mouse ovarian surface epithelial cells

Lei Lv,[1,†] Tianwei Zhang,[1,†] Qiyi Yi,[1] Yun Huang,[1] Zheng Wang,[1] Heli Hou,[1] Huan Zhang,[1] Wei Zheng,[1] Qiaomei Hao,[1] Zongyou Guo,[2] Howard J. Cooke[1,3] and Qinghua Shi[1,*]

[1]Hefei National Laboratory for Physical Sciences at Microscale and School of Life Sciences; University of Science and Technology of China; Hefei, China; [2]Department of Dermatology; Brigham and Women's Hospital and Harvard Skin Disease Research Center; Harvard Institutes of Medicine; Boston, MA USA; [3]MRC Human Genetics Unit and Institute of Genetics and Molecular Medicine; University of Edinburgh; Western General Hospital; Edinburgh, UK

[†]These authors contributed equally to this work.

Keywords: ovarian cancer, cytokinesis failure, tetraploid cells, chromosome mis-segregation, aneuploidy

Abbreviations: MOSECs, mouse ovarian surface epithelial cells; FISH, fluorescence in situ hybridization; CIN, chromosomal instability

Most ovarian cancers originate from the ovarian surface epithelium and are characterized by aneuploid karyotypes. Aneuploidy, a consequence of chromosome instability, is an early event during the development of ovarian cancers. However, how aneuploid cells are evolved from normal diploid cells in ovarian cancers remains unknown. In the present study, cytogenetic analyses of a mouse syngeneic ovarian cancer model revealed that diploid mouse ovarian surface epithelial cells (MOSECs) experienced an intermediate tetraploid cell stage, before evolving to aneuploid (mainly near-tetraploid) cells. Using long-term live-cell imaging followed by fluorescence in situ hybridization (FISH), we demonstrated that tetraploid cells originally arose from cytokinesis failure of bipolar mitosis in diploid cells, and gave rise to aneuploid cells through chromosome mis-segregation during both bipolar and multipolar mitoses. Injection of the late passage aneuploid MOSECs resulted in tumor formation in C57BL/6 mice. Therefore, we reveal a pathway for the evolution of diploid to aneuploid MOSECs and elucidate a mechanism for the development of near-tetraploid ovarian cancer cells.

Introduction

Ovarian cancer is the most lethal gynecological malignancy and the fifth leading cause of cancer deaths among women, with five-year survival rates of only 45%.[1] Epithelial ovarian carcinomas (EOC), which derive from the ovarian surface epithelium (OSE), represent approximately 90% of all human ovarian malignant neoplasms.[2] Epidemiological data indicate that the risk of EOC increases with the number of ovulatory events.[3,4] It is proposed that the repetitive rupture and resulting cell proliferation in postovulatory repair of the ovarian surface epithelium produce accumulating genetic aberrations in the epithelial cells that ultimately lead to tumor formation.[3,4] This incessant ovulation hypothesis was supported by several groups who reported that spontaneous transformation of rat ovarian surface epithelial cells occurred after prolonged subculture.[5,6] Thus, passaging cells in culture mimics the proliferation of ovarian surface epithelium after ovulation. Afterwards, a syngeneic mouse model was established by continuous passaging and spontaneous transformation of mouse ovarian surface epithelial cells from C57BL/6 mice, which represented an excellent model used to characterize molecular and cellular events associated with ovarian carcinogenesis.[7,8]

Aneuploidy, the condition in which a cell gains or losses of chromosomes, arises as a consequence of chromosomal instability (CIN). It is a common characteristic of many human cancers, including ovarian cancers.[9,10] The degree of aneuploidy correlates with malignancy of tumor, risks of metastasis and poor prognosis in ovarian cancers.[11-13] Importantly, formation of aneuploid cells is found to be an early event in the development of ovarian cancer, underscoring the pivotal role of aneuploidy in cancer initiation.[14] Multiple mechanisms, including defects in genes ensuring the fidelity of chromosome replication and segregation, compromised spindle assembly checkpoint, persistent merotelic attachment and multipolar mitosis, have been proposed to be responsible for aneuploidy and /or CIN.[15,16] Notably, a long-standing hypothesis is that the transient tetraploid intermediate could facilitate the development of aneuploidy, cellular transformation and tumor formation.[17-21] Tetraploidization has been identified to precede aneuploidy during the development of many solid tumors, such

*Correspondence to: Qinghua Shi; Email: qshi@ustc.edu.cn
Submitted: 05/16/12; Revised: 06/19/12; Accepted: 06/20/12
http://dx.doi.org/10.4161/cc.21196

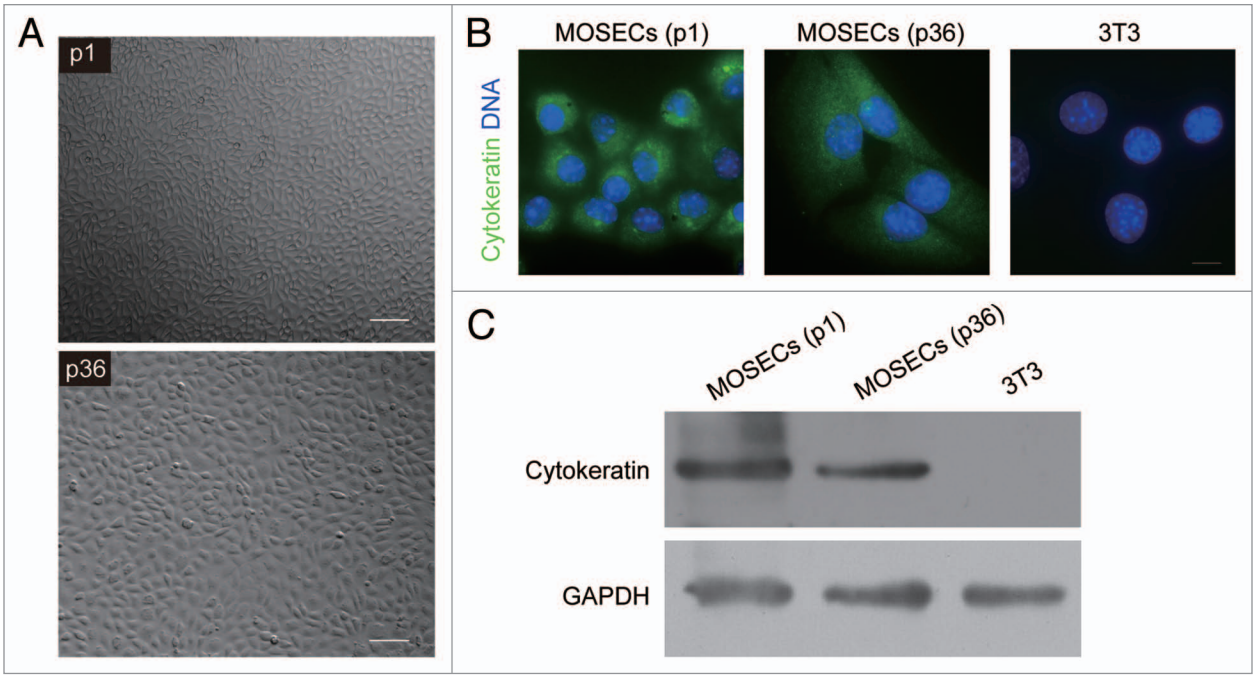

Figure 1. Establishment and characterization of spontaneously immortalized MOSECs. (A) Morphology of cultured MOSECs at early (p1) and late passage (p36). (B and C) Characterization of MOSECs by immunofluorescence staining (B) and western blotting (C) using cytokeratin antibodies, the murine fibroblast 3T3 cells were used as negative control. Bars = 100 μm (A) and 10μm (B).

as Barrett esophagus, cervical tumor and colon cancer.[22-24] It has been reported that the risk of ovarian cancer goes up with age,[25] and the percentage of tetraploid ovarian surface epithelial cells is significantly higher in older than in younger women.[26] Furthermore, many ovarian cancers are near-tetraploid.[10,27] Thus the tetraploid cells are associated with ovarian cancer development. Nevertheless, the origin of aneuploid cells as well as their relationships with tetraploid intermediates during ovarian cancer formation is still unrevealed.

In the present study, we utilized long-term live-cell imaging followed by fluorescence in situ hybridization (FISH) to examine the origins of aneuploid cells in spontaneously immortalized and transformed MOSECs. Our results highlight the important role of tetraploid intermediates in the development of aneuploid ovarian cancer.

Results

Establishment of spontaneously immortalized mouse ovarian surface epithelial cells (MOSECs). A mouse syngeneic model of ovarian cancers was established by continuous subculture of primary MOSECs in vitro according to the method described previously.[7,8] Before passage 6 (p6), the cells grew slowly and were split at a ratio of 1:3 every 2 weeks. They show a typical cobblestone-like appearance (**Fig. 1A**). After passage 6, however, the cells had a faster growth rate and were subcultured at a ratio of 1:10 every 4 to 7 d for more than 30 passages. This finding is consistent with the observation reported on spontaneous immortalization of MOSECs.[7] Compared with early passage cells, late passage cells were flatter and larger (**Fig. 1A**). Immunofluorescence staining and western blot analysis indicated that both early (p1) and late passage (p36) cells were cytokeratin-positive (**Fig. 1B and C**), indicating that the cells were of epithelial origin.

Immortalized aneuploid MOSECs are tumorigenic in vivo. To determine whether the MOSECs we generated were tumorigenic, MOSECs from different passages were injected intraperitoneally into normal female C57BL/6 mice and the animals were monitored for 2 to 4 mo after injection. At the time of sacrifice, no visible tumors or ascites were observed in the mice injected with early passage (p9) cells (n = 8) or PBS (n = 10) (**Table S1**). In contrast, all three mice injected with late passage (p37) cells were found to have multiple small nodules from 1 to 3 mm diameters on the surface of the peritoneum and intestine two months later (**Fig. 2A**). Hematoxylin staining confirmed the hyperplasia on the surface of intestines (**Fig. 2B**). Mitotic figures and giant nuclei were also noted within the tumor area (**Fig. 2B**). Similarly, all the four mice sacrificed four months after injection developed tumors, three of which had hemorrhagic ascites (**Table S1**). Notably, histopathological analysis of the nodules by immunohistochemistry with cytokeratin and PCNA antibodies demonstrated that they were of epithelial origin and proliferated actively (**Fig. 2C**). Therefore, the late (which were almost all aneuploid as described below) rather than early passage MOSECs were able to induce tumorigenesis after being injected into mice intraperitoneally.

Tetraploid cells precede aneuploid cells during spontaneous transformation of MOSECs. To understand cytogenetic changes during spontaneous transformation of MOSECs, the cells at different passages were subjected to DNA content analysis by flow

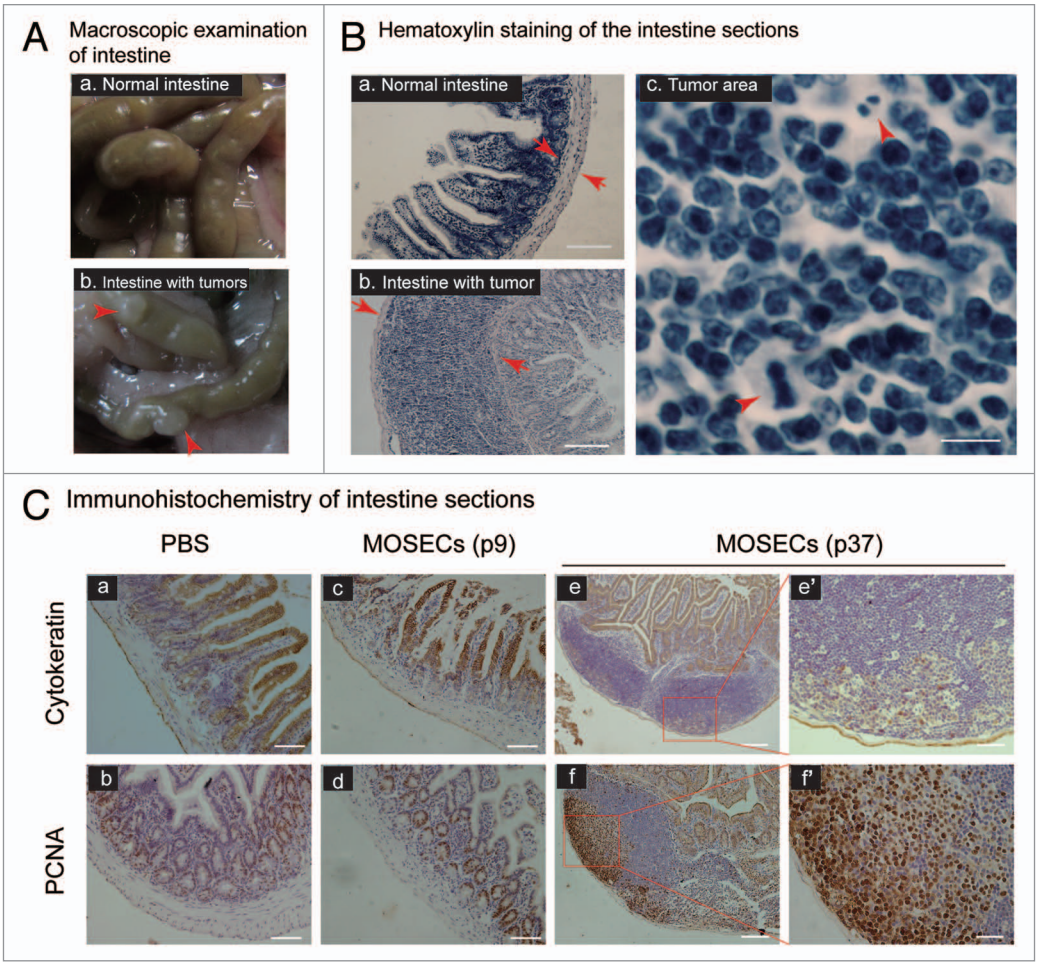

Figure 2. Tumorigenicity of late passage MOSECs. (A) Macroscopic images of intestines from mice injected with PBS (a) or MOSECs at p37 (b). The mice were sacrificed 2 mo after injection. Arrowheads show tumors on surface of the intestines. (B) Hematoxylin staining of sections of intestine from a mouse injected with PBS (a) and intestines with a nodule from a mouse injected with MOSECs at p37. Arrows show the wall of intestines. (c) Mitotic figures (arrowheads) seen in a tumor section. Bar = 100 μm for (a and b) and 10 μm for (c). (C) Immunohistochemistry with antibodies against cytokeratin and PCNA for the identification of cell identity and cell proliferation, respectively. Bar = 100 μm for (a–d), 200 μm for (e and f), 50 μm for (e′ and f′).

cytometry, chromosome numeration in metaphase cells by chromosome counting and in interphase cells by FISH using chromosome-specific probes. Flow cytometry analyses showed that MOSECs with a diploid DNA content decreased from 43.2% at passages 9 (p9) to 39.9% at p19, and finally disappeared at p36, whereas those with a tetraploid DNA content increased from 25.5% at p9 to 30.5% at p19, and reached a plateau at 48.9% at p26 then decreased to 42.0% at p36; accordingly, the cells with a octoploid DNA content became obvious at p26 and p36 (**Fig. 3A**). These analyses indicate that a fair amount of tetraploid cells are generated during spontaneous transformation of MOSECs.

Because flow cytometry fails to distinguish between cells with only a few chromosome gains or losses (e.g., near-diploid vs. diploid cells, near-tetraploid vs. tetraploid cells, etc.), to carefully characterize cytogenetic changes of MOSECs during the spontaneous transformation, we performed chromosome counting in metaphase spreads from cells at different passages. As shown in **Figure 3B**, 83.3% of the cells at passage p6 were diploid, with 8.3% being tetraploid cells. With cell passaging, the proportion of diploid cells decreased, while tetraploid cells increased. At p19, the diploid cells fell to 49.3%, and tetraploid cells reached 29.3%. By p26, 22.9% of the cells were tetraploid, and 71.0% were near-tetraploid, with 47.3% being hypo-tetraploid (containing 70–79 chromosomes) and 23.7% being hyper-tetraploid (containing 81–94 chromosomes). When passaged to p35, 98.0% of MOSECs became aneuploid, of which 90.0% were near-tetraploid (**Fig. 3B**). The fact that the proportion of tetraploid cells increased during the early passages then gradually decreased later on, and that the increase of tetraploid cells preceded the increase of near-tetraploid cells indicates that tetraploid cells would be intermediates from diploidy to near-tetraploid aneuploidy transition.

To confirm our findings above, FISH analysis using chromosome-specific centromere probes (chromosome 2 and X), which enable the detection of chromosome composition in a large number of interphase cells, was performed (**Fig. 3C**). The ploidy status of cells following FISH was arbitrarily assigned based on the number of FISH signals for chromosome 2 and X, as described

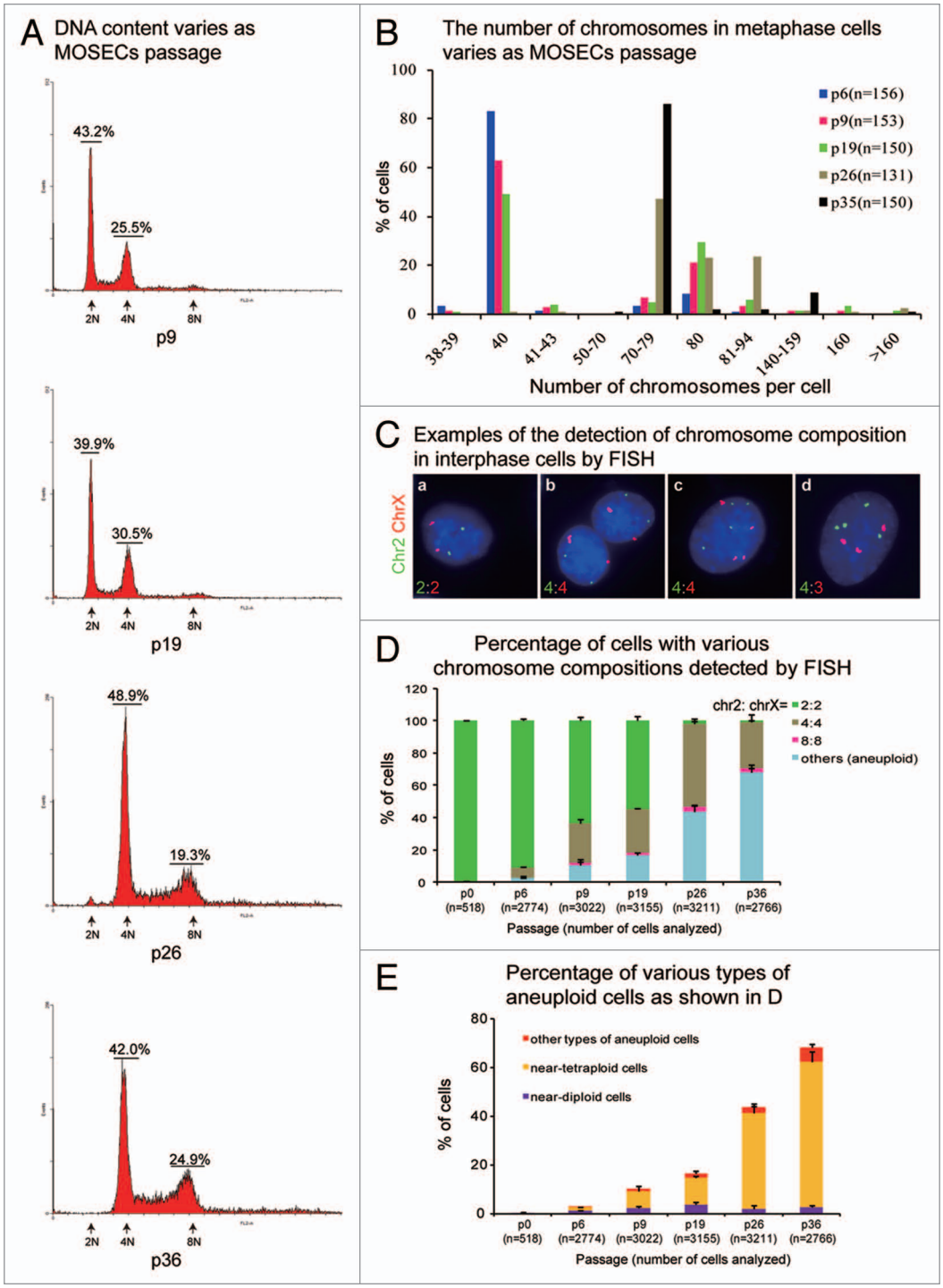

Figure 3. Genetic evolution of MOSECs. (A) DNA content varies as MOSECs passage detected by FACS. Results shown are from one of three independent experiments with similar results. (B) The number of chromosomes in a cell varies as MOSECs passage determined by chromosome counting in metaphase spreads. (C) Representative images of interphase mono- (a, c and d) and bi-nucleated MOSECs (b) showing various chromosome compositions detected by FISH using centromeric probes specific to chromosome 2 (green) and X (red). The numbers shown in the lower left corner of each image are the copy number of chromosome 2 (green) to X (red). (D) Quantification of the MOSECs with various copies of chromosome 2 and X at different passages. Others: the chromosome composition is different from those indicated. Taking into account the results of flow cytometry analysis and chromosome counting, here the cells containing two, four and eight FISH signals for both chromosome 2 and X are called di-, tetra- and octo-ploidy, respectively; otherwise, the cells are considered as aneuploidy. (E) Quantification of various types of aneuploid cells as shown in (D). Ploidy status of a cell is determined according to the description in Materials and Methods. Mean ± SD, from three independent experiments.

in Materials and Methods. As shown in **Figure 3D**, 99.2% of MOSECs at p0 were diploid. With cell passaging, the proportion of diploid cells gradually decreased to 91.1% at p6, 63.5% at p9, 54.7% at p19, 2.1% at p26 and 1.0% at p36, accompanied by the variation of tetraploid cells (6.1% at p6, 24.1% at p9, 27.0% at p19, 51.2% at p26 and 28.3% at p36) and steadily increase of aneuploid cells (2.6% at p6, 10.3% at p9, 16.6% at 19, 43.8% at p26 and 68.3% at p36). What's more, most of the aneuploid cells were near-tetraploid, which increased from 54.8% at p6 to 87.4% at p36 in the aneuploid cell population (**Fig. 3E**). Together with the data from flow cytometry analysis and chromosome counting, the data presented here clearly show that during the spontaneous transformation, the diploid MOSECs experienced an intermediate tetraploid cell stage before evolving to aneuploid cells.

Most aneuploid cells are derived from tetraploid cells via chromosome mis-segregation in bipolar and multipolar mitoses. To delineate genesis of aneuploid MOSECs, the division of MOSECs at p8, from which onwards aneuploid cells started to increase rapidly, was monitored by long-term live-cell imaging followed by FISH analysis for chromosome compositions in daughter cells (**Fig. 4A–E**). Immediately after live-cell imaging, we fixed the cells and performed FISH using chromosome 2- and X-specific probes. The copy numbers for a specific chromosome in daughter cells could be directly detected by FISH, and those in their parental cells were determined based on the total number of FISH signals in all of its daughter cells divided by 2 if it had divided once or by 4 if it had divided twice, because chromosomes duplicated once per division. The ploidy status was determined as described above.

In total, 35 aneuploid daughter cells were observed to arise from euploid parental cells during time-lapse imaging, with five (14.3%) being near-diploid and 30 (85.7%) being near-tetraploid cells. Of the five near-diploid daughters, two (**Fig. 4A**, panels a and b) were generated from a diploid cell undergoing bipolar mitosis with nondisjunction of a chromosome 2 (**Fig. 4A**), and the other three were generated from tetraploid cells undergoing multipolar mitosis with completion of cytokinesis (**Fig. 4B**). However, all 30 near-tetraploid daughters were generated from tetraploid parental cells, six of which (6/30, or 20.0%) resulted from multipolar mitosis in which cytokinesis often partially completed (4 out of 6, **Figure 4C**). The remaining 24 (24/30, or 80.0%) were derived from chromosome mis-segregation in bipolar mitosis of bi- (4/24, or 16.7%, **Figure 4D**) or mono-nucleated tetraploid parental cells (20/24, or 83.3%, **Figure 4E**). Taken together, 94.3% (33/35) of aneuploid progenies were derived from tetraploid parental cells that underwent bipolar (24/33, or 72.7%) or multipolar divisions (9/33, or 27.3%) with chromosome mis-segregation (**Fig. 4F**). These direct data unequivocally indicate for the first time that most aneuploid MOSECs are derived from tetraploid parental cells undergoing either bipolar or multipolar mitoses.

The initial tetraploid MOSECs result from cytokinesis failure of bipolar mitosis in mononucleated diploid cells. Given that tetraploid cells play a pivotal role in the generation of aneuploid MOSECs, we next traced the origins of the tetraploid cells using long-term live-cell imaging followed by FISH analysis as described above. A total of 481 newly generated tetraploid cells were successfully detected by FISH following live-cell imaging, with 143 being binucleated and 338 being mononucleated (**Fig. 5E**). All of the 143 binucleated tetraploid cells resulted from cytokinesis failure of bipolar mitosis in mononucleated diploid cells. In mononucleated diploid cells undergoing bipolar mitosis, 85.9% (873/1,016) of them completed cytokinesis and produced two mononucleated diploid cells (**Fig. 5A**), the rest (143/1,016, or 14.1%) failed to complete cytokinesis. The cells ending up with cytokinesis failure seemed to have initiated mitosis, congressed and lined up their chromosomes at metaphase plate and separated their chromosomes normally. However, these cells exited from mitosis inappropriately, with failure of cytokinesis completion leading to the formation of binucleated cells with doubled chromosome numbers (**Fig. 5B**). The 338 newly generated mononucleated tetraploid cells were generated from bipolar mitosis of previously existing tetraploid cells, of which 64 (26.9%) were from binucleated cells (**Fig. 5C**) and 274 (73.1%) were from mononucleated ones (**Fig. 5D**). As shown in **Figure 3D**, when culture of MOSECs initiated, tetraploid cells were very rare (0.4% at p0), so these previously existing tetraploid cells during live-cell imaging were considered to also have originally resulted from diploid cells by incomplete cytokinesis. Moreover, we did not observe cell fusion and mitotic slippage during live-cell imaging. Besides, neither paired chromosomes nor paired FISH signals were found in metaphase spreads or interphase cells, excluding the possibility of endoreduplication. Also FISH analyses in interphase cells regarding ploidy status and cell types revealed that cytokinesis failure occurred frequently in diploid cells at different passages but not in tetraploid cells (**Fig. S1**). This led to the gradual decrease of diploid cells and accumulation of tetraploid or aneuploid cells. Therefore, cytokinesis failure was the key event for transition from diploidy to tetraploidy.

Altogether, these data showed that cytokinesis failure of bipolar mitosis in mononucleated MOSECs would lead to binucleated tetraploid cells, which could generate mononucleated tetraploid cells in a subsequent bipolar mitosis, and that the proliferation of mononucleated tetraploid cells contributed to the accumulation of tetraploid cells in the population. However, some of these tetraploid cells underwent bipolar or multipolar mitosis with chromosome mis-segregation and produced aneuploid (mainly near-tetraploid) cells. These aneuploid cells could cause tumor formation after intraperitoneal injection into mice (**Fig. 6**).

Discussion

In ovarian carcinomas, severely aneuploid karyotypes are prevalent, and aneuploidy is associated with disease initiation, progression and aggression.[14,28-30] However, how the aneuploid cells are evolved from normal diploid cells in ovarian cancer is still unknown. Because of the inadequate supply of human tissues in the early disease stages of ovarian cancer, researchers have set up immortalized human ovarian surface epithelial cells as a model in order to study the events related with the early steps in ovarian tumorigenesis. However, these cells were engineered to artificially express ectopic human telomerase reverse transcriptase (hTERT)

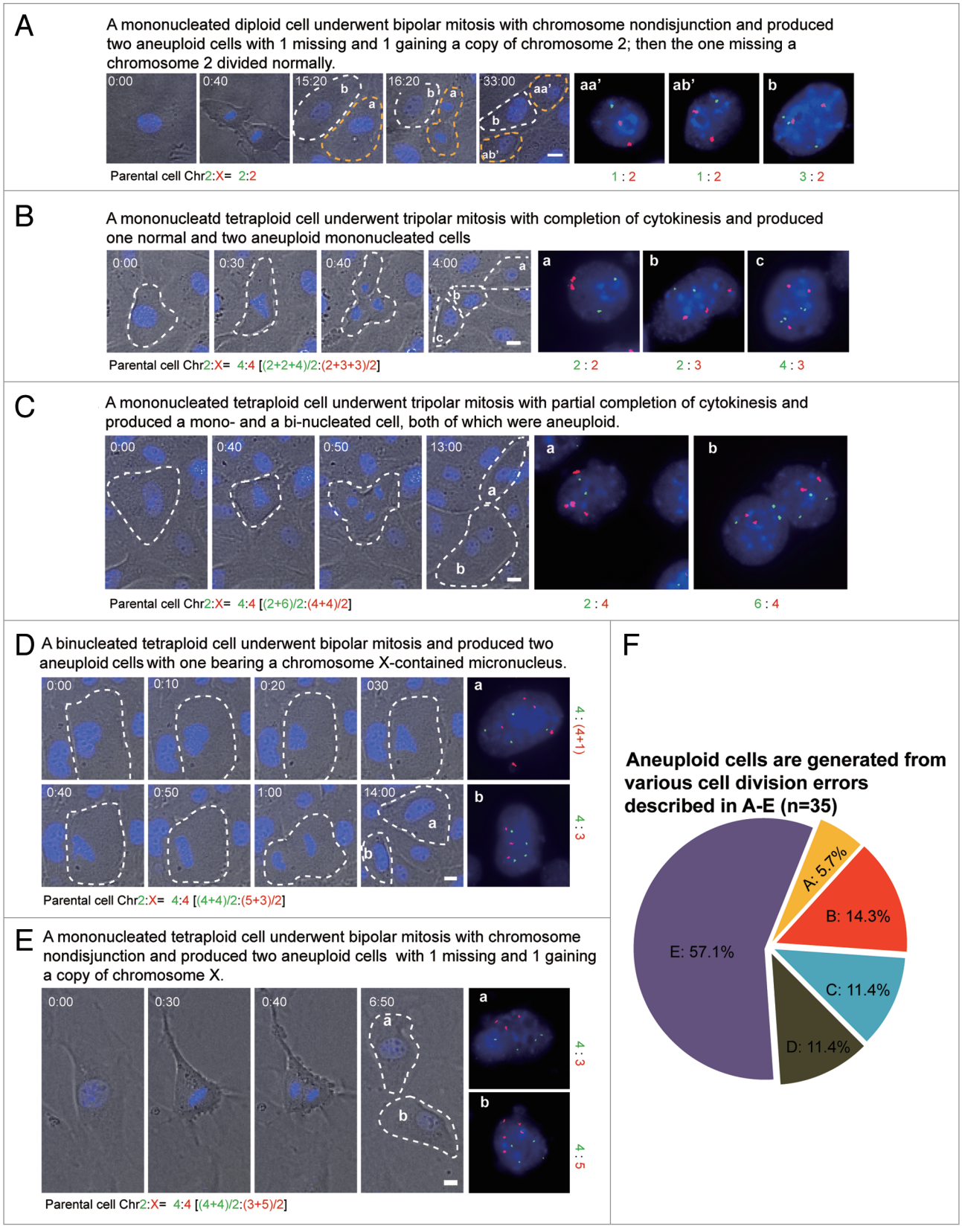

Figure 4. For figure legend, see page 2870.

Figure 4 (See previous page). Most aneuploid cells are resulted from tetraploid cells undergoing bipolar mitosis with chromosome mis-segregation or multipolar mitoses. (A–E) Divisions that generate aneuploid cells are determined by FISH analyses of daughter cells for chromosome segregation following long-term live-cell imaging. The number of chromosome 2 and X in a cell presenting in the last frame of time-lapse imaging was directly assayed by FISH using chromosome 2 (green) and X-specific probes (red), while that in a mother cell was calculated based on the total number of FISH signals for each chromosome analyzed in all of its daughter cells divided by 2 if it has divided once. Representative serial images show that (A) a mononucleated diploid cell underwent a bipolar mitosis with nondisjunction of chromosome 2 and produced two daughter cells with 1:2 (yellow circle) and 3:2 (white circle) for chromosome 2: X and the one missing a copy of chromosome 2 (yellow circle) completed another round of bipolar mitosis; (B) a mononucleated tetraploid cell underwent a tripolar mitosis with completion of cytokinesis and produced three daughter cells with chromosome 2: X compositions of 2:2, 2:3 and 4:3, respectively; (C) a mononucleated tetraploid cell underwent a tripolar mitosis with partial completion of cytokinesis, and produced a mono- and a bi-nucleated cell with 2:4 and 6:4 for chromosome 2: X, respectively; (D) a binucleated tetraploid cell underwent a bipolar mitosis and produced two daughter cells with chromosome 2: X compositions of 4:5 (one chromosome X present in micronucleus) and 4:3; (E) a mononucleated tetraploid cell underwent a bipolar mitosis with nondisjunction of chromosome X and produced two daughter cells with 4:3 and 4:5 for chromosome 2: X, respectively. Green and red spots are FISH signals for chromosome 2 and X, respectively. Time is indicated in hours:minutes. Bar = 10 μm. (F) Quantification of divisions that produced aneuploid cells. n, the number of aneuploid cells analyzed.

in combination with SV40 T-antigen or human papillomavirus E6/E7 transduction,[31,32] which may not simulate the true process of tumorigenesis. Here, a spontaneously transformed MOSECs model was established to study the cytogenetic changes in the early development of ovarian cancer, which demonstrated that transient tetraploid intermediates facilitate the development of aneuploidy and thus result in cellular transformation and tumor formation.

During the process of transformation, we observed that the fraction of diploid cells decreased, while the percentage of tetraploid increased from p6 to p19 (**Fig. 3B and D**). Tetraploidization in our model mimics the increased percentage of tetraploid cells in old women[26] who have accumulated numbers of ovulation events, resulting in proliferation of ovarian surface epithelial cells and high risk of ovarian cancers.[25] Combining long-term live-cell imaging with FISH, we demonstrated that cytokinesis failure was responsible for the transition from diploidy to tetraploidy of MOSECs (**Fig. 5B**). Cytokinesis failure has been suggested as a possible cause of CIN and cancer. Dominant mutation of *adenomatous polyposis coli* (APC) in human colorectal cancer[33] and loss of heterozygosity at Polo kinase 4 (Plk4) in human hepatocellular carcinomas[34] have been shown to induce cytokinesis failure, which represents the first step in the onset of genomic instability and cancer development. Many proteins regulating cytokinesis were mutated or aberrantly expressed in various human cancers.[35] Here, the mechanisms by which the diploid MOSECs fail to complete cytokinesis remain to be determined.

Tetraploidy has been proposed as a genetically unstable intermediate, which can result in aneuploidy and cancer.[20,36,37] We observed that the frequency of tetraploid cells peaked at p19 but decreased with the further passages (**Fig. 3B**), while the fraction of aneuploid cells increased steadily with continuous subculturing (**Fig. 3B and D**), confirming that tetraploidy was a transient intermediate and associated with the formation of aneuploid cells during spontaneous transformation of MOSECs. Moreover, using long-term live-cell imaging followed by FISH, we demonstrated that most aneuploid cells were derived from tetraploid ones (**Fig. 4F**), supporting the idea that tetraploidization is the initial step toward aneuploidy and tumor.

Aneuploidy from a tetraploid precursor was thought to arise from either multipolar mitosis[38] or progressive chromosomal loss in bipolar mitosis.[39] However, how aneuploid cells are derived from tetraploid cells has not been well confirmed in live cells. Utilizing long-term live-cell imaging followed by FISH, we observed that 27.3% of the aneuploid daughters of tetraploid parental cells resulted from multipolar mitosis; the remaining 72.7% were from bipolar mitosis (**Fig. 6**), indicating that bipolar mitosis is more prevalent than multipolar mitosis to produce aneuploid cells in our MOSECs model. Given that most progenies of multipolar mitosis are inviable,[39] evolution from tetraploidy to aneuploidy during spontaneous transformation of MOSECs was mainly attributed to bipolar mitosis. We also observed that tetraploid MOSECs undergoing bipolar mitosis initiated a multipolar spindle that ultimately became bipolar on occasion (**Fig. 4D**). Such transient multipolar spindles have been demonstrated to increase the occurrence of merotely (microtubules emanating from different poles attach to a single kinetochore), which, if not corrected, causes chromosome mis-segregation.[39-41] Indeed, the incidence of chromosome mis-segregation was significantly higher in tetraploid cells than that in their diploid counterparts during bipolar divisions (**Fig. S2**).

Cytogenetic analyses in this study demonstrated that late passage (p36) aneuploid cells were predominantly near-tetraploid (**Fig. 3B and E**), which induced tumors after injection into mice (**Fig. 2A**). Consistently, human ovarian surface epithelial cells became near-tetraploid in culture about 10 passages after immortalization with hTERT and SV40 T-antigen,[32] and some ovarian tumors are near-tetraploid.[10,27] It has been reported that near-tetraploid ovarian tumors possessed a much higher level of numerical chromosomal instability than near-diploid and near-triploid tumors[27] and were accompanied by a more frequent metastases and a significantly worse prognosis,[42,43] underscoring the importance of near-tetraploidy.

In summary, based on the syngeneic mouse model of ovarian cancer, we, for the first time, provide direct evidence that tetraploid cells arising from cytokinesis failure of diploid cells give rise to aneuploid daughters through chromosome mis-segregation during both bipolar and multipolar mitosis in live cells (**Fig. 6**). Our elucidation of how aneuploid cells are generated from normal diploid cells during spontaneous transformation of MOSECs may provide answer to many questions regarding the induction of ovarian tumor. Furthermore, this "diploidy-tetraploidy-aneuploidy" pathway may help to understand the cellular development of cancers, which had a premalignant tetraploid stage (e.g., colon cancer, Barrett's esophagus and cervical cancer) and the mechanism of some bacteria-initiated tumors.[44,45]

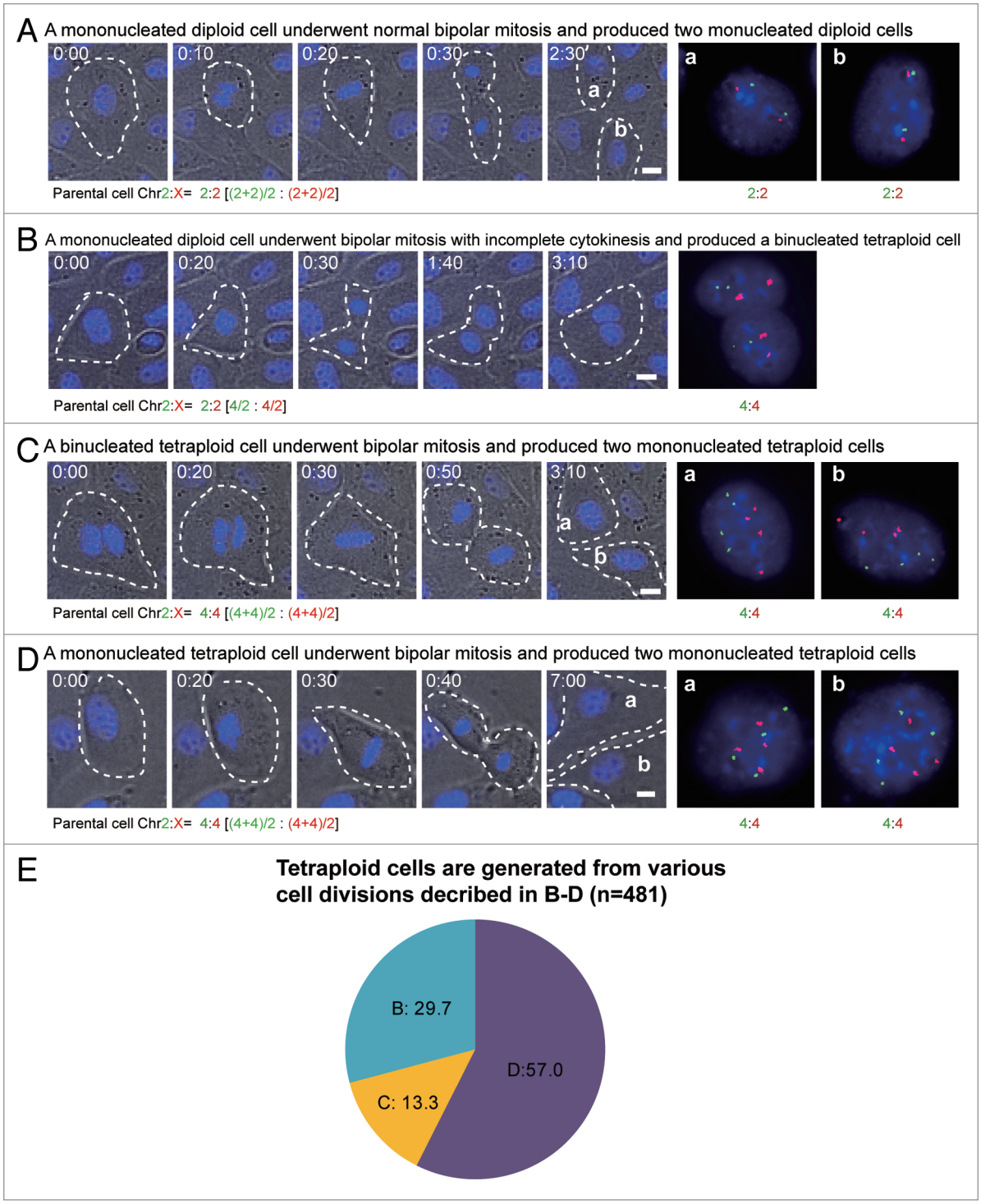

Figure 5. The initial tetraploid MOSECs originate from cytokinesis failure of mononucleated diploid cells. (A–D) Divisions generating tetraploid cells are detected by FISH analyses of the daughter cells for chromosome composition following long-term live-cell imaging. Chromosome composition of cells is determined as in **Figure 4**. Green and red spots are FISH signals for chromosome 2 and X, respectively. Time is indicated in hours:minutes. Bar = 10 μm. Representative serial images showing that (A) a mononucleated diploid cell underwent normal bipolar mitosis and produced two mononucleated diploid cells; (B) a mononucleated diploid cell underwent bipolar mitosis with incomplete cytokinesis and produced a binucleated tetraploid cell; (C) a binucleated tetraploid cell underwent bipolar mitosis and produced two mononucleated tetraploid cells; (D) a mononucleated tetraploid cell underwent bipolar mitosis and produced two mononucleated tetraploid cells. (E) Quantification of divisions that produced tetraploid cells. n, the number of tetraploid cells analyzed.

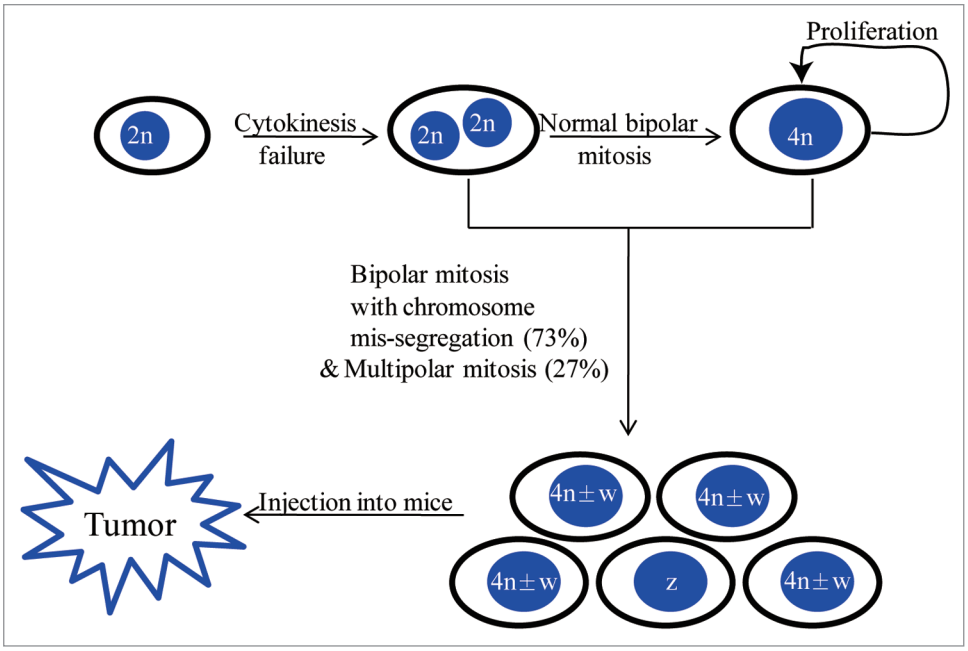

Figure 6. A schematic diagram summarizing the genetic evolution of tumorigenic MOSECs. Diploid (2n) MOSECs undergo bipolar mitosis with cytokinesis failure leading to binucleated tetraploid (2 x 2n) cells, which generate mononucleated tetraploid (4n) cells through normal bipolar mitosis. Subsequent proliferation of mononucleated tetraploid cells results in more tetraploid ones. However, some of these tetraploid cells undergo bipolar or multipolar mitosis with chromosome mis-segregation and produce aneuploid (mainly near-tetraploid) cells. These aneuploid cells cause tumor formation after intraperitoneal injection into C57BL/6 mice. (4n ± w) represents near tetraploidy, and z represents other types of aneuploidy.

Materials and Methods

Cell isolation and culture. Mouse ovarian surface epithelial cells (MOSECs) were isolated as reported in references 7 and 8. Briefly, ovaries were removed from female, 8-week-old C57BL/6 mice aseptically and incubated in 0.2% trypsin-EDTA (Gibco 25200, diluted with 1 x PBS) for 25 min at 37°C to selectively isolate surface epithelial cells. Cells were collected by centrifugation at 120 g for 7 min and then plated in a P30 dish in MOSEC medium, which consists of Dulbecco's modified Eagle's medium (DMEM, Gibco 12800) supplemented with 4% fetal bovine serum (Hyclone SV30087.02), 1% insulin-transferrin-selenium (Gibco 41400–045), 100 U/ml penicillin and 100 μg/ml streptomycin (Gibco 15140–122). Hydrocortisone (0.5 μg/ml, Sigma H0888) and murine epidermal growth factor (2 ng/ml, Invitrogen 53003018) were added to the medium for cells before passage 6.

Flow cytometry analysis. To prepare cells for flow cytometry analysis, MOSECs were trypsinized and washed once with phosphate-buffered saline (PBS), and fixed by re-suspending the pellet in ice-cold 100% ethanol with gentle agitation, then the cells were kept at -20°C until use. Before flow cytometry analysis, the cells were re-suspended in 50 μg/ml propidium iodide and 100 μg/ml RNase A solution, and incubated at 37°C for 30 min. Flow cytomery analysis were performed on BD FACS caliber with CELLQUEST software, and statistics were handled with WinMDI.

Metaphase chromosome preparation. When the MOSECs proliferated at a log phase, colcemid was added to the medium to a final concentration of 0.05 μg/ml 2 h before cell harvesting.[8] The cells were harvested by trypsinization and hypotonically treated with 75 mM KCl for 15 min then fixed in methanol: acetic acid (3:1). After three changes of the fixative, the chromosome preparations were made by dropping the cell suspension onto cold slides, which were then air-dried. Then the slides were stained with Giemsa.

Fluorescence in situ hybridization (FISH). Murine chromosome 2-centromere specific BAC clone (clone ID 49N22) was purchased from Invitrogen (96022), and the DNA was extracted using Wizard Plus VS Minipreps DNA Purification System (Promega A1460). Murine chromosome X-centromere specific *E.coli* XLI-blue clone (clone ID DXWas70) was used as previously described.[46] Probes were labeled with either SpectrumGreen dUTP (Vysis 30–803200, for chromosome 2) or SpectrumOrange dUTP (Abbott 02N33–50, for chromosome X) by random priming using the BioPrime DNA Labeling System (Invitrogen 18094–011). Hybridizations were performed as previously described.[47] For cells after live-cell imaging, permeablization with NP-40 was extended to 30 min. Slides after FISH were examined using an Olympus BX-61 fluorescence microscope fitted with band pass filters detecting Hoechst, SpectrumOrange and SpectrumGreen. Images were captured with a CCD camera (Retiga Exi FAST, Qimaging) using Image-Pro Plus software (Media Cybernetic, Inc.).

Criteria used for the analysis of FISH samples were followed as stated in reference 21. Ploidy status of a cell is determined arbitrarily based on the number of FISH signals for both chromosomes analyzed as described in reference 48. Specifically, the

number of FISH signals for chromosome 2 and X in a cell is denoted by A and X, respectively. When the sum of absolute values for (A-2) and (X-2) equal 0 in a cell, indicating that the cell contains two copies of chromosome 2 and X, the cell is considered as a diploid cell. When the sum equals 1, indicating that the cell misses or gains a copy of either chromosome 2 or X, then the cell is considered as a near-diploid cell, e.g., 1:2 and 3:2 for chromosome 2 to X and vice versa. When the sum of absolute values for (A-4) and (X-4) equal 0 in a cell, indicating that the cell contains 4 copies of both chromosome 2 and X, then the cell is considered as a tetraploid cell. When the sum equal 1 or 2, then the cell is considered as a near-tetraploid cell, e.g., 3:3, 3:5, 4:2, 4:3, 4:5, 4:6 and 5:5 for chromosome 2 to X and vice versa. When the sum of absolute values for (A-8) and (X-8) equal 0 in a cell, indicating that the cell contains 8 copies of both chromosome 2 and X, the cell is considered as an octoploid cell. Cells with a chromosome composition other than those mentioned above are considered as other types of aneuploid cells. As shown in **Figure 3E**, other types of aneuploid cells only consist of a very small proportion (< 6%). Interestingly, ploidy status of cells determined following these criteria is consistent with those from flow cytometry analysis (**Fig. 3A**) and chromosome counting (**Fig. 3B**), indicating that the criteria used for the determination of chromosome ploidy of cells after FISH are feasible.

Chromosome composition of cells undergoing long-term live-cell imaging was determined as follows: The number of a chromosome studied in a cell presenting in the last frame of time-lapse imaging was directly assayed by FISH using chromosome-specific probes, while that in a mother cell was calculated based on the total number of FISH signals for the chromosome analyzed in all of its daughter cells divided by 2 if it has divided once or by 4 if it has divided twice because chromosomes duplicated once per division.

Immunofluorescence. Cells grown on coverslips were fixed in 4% paraformaldehyde for 10 min at room temperature, washed with TBST (0.1% Triton in Tris-buffered saline) for 3 x 5 min. Then the cells were blocked with 2% bovine serum albumin (Sigma A7906) in TBST for 1h, and sequentially incubated with mouse anti-pan cytokeratin antibody (Sigma C1801; 1:100) and AF488 conjugated donkey anti-mouse antibody (Molecular Probes A21202; 1:200). All incubations were performed at 37°C for 2 h, and nuclei were counterstained with DAPI.

Western blot analysis. Lysates from passage 1 (p1) and passage 36 (p36) MOSECs and 3T3 cells were separated on 12% SDS polyacrylamide gels, and the proteins were then transferred to nitrocellulose membranes (Amersham Biosciences, RPR303D). The membranes were blocked in TBST (0.5% Tween-20 in Tris-buffered saline) containing 5% nonfat milk powder for 1 h, incubated overnight with a mouse anti-pan cytokeratin monoclonal antibody (1:200), and a mouse anti-GAPDH monoclonal antibody (Millipore MAB374; 1:1000) in TBST at 4°C, then washed three times (10 min each) with TBST. The membranes were then incubated for 1 h with alkaline phosphatase (AP)-conjugated anti-mouse IgG (Promega S372B; 1:1000) at room temperature.

Live-cell imaging and image analysis. Cells grown on gridded coverglass bottom dishes (MatTek Corporation) were stained with 400 ng/ml Hoechst 33342 (Molecular Probes) for 30 min at 37°C, washed with PBS and culture medium (3 times each), and maintained in culture medium containing 20 ng/ml Hoechst 33342. Then, images were acquired automatically using a Nikon TE2000E inverted microscope equipped with the Nikon Perfect Focus system, a linearly encoded stage (Proscan, Prior) and a cooled CCD camera (Orca R^2, Hamamatsu). The microscope was controlled by NIS-Elements Advanced Research (Nikon) software and housed in a custom-designed 37°C chamber with a secondary internal chamber that delivered humidified 5% CO_2. Fluorescence and phase contrast images were captured at multiple locations every 10 min for a period of 48 h with a 20x Plan Apo objective. Immediately after live-cell imaging, the cells were fixed in methanol: acetic acid (3:1) and kept at -20°C before FISH.

Images from long-term live-cell imaging were analyzed frame by frame manually as reported in reference 21. Multipolar divisions were defined as chromosomes segregating toward three or more directions during anaphase or telophase, and subsequently producing three or more nuclei. Cells that underwent bipolar mitosis were analyzed for the presence of lagging chromosomes or chromosomal bridges as described in reference 49. Briefly, lagging chromosomes were indentified as the Hoechst-positive materials observed in the midzone in anaphase or telophase, or in the cytoplasmic bridge during the progression of cytokinesis. Chromosomal bridges were indentified as the Hoechst-positive materials that extended continuously between the two masses of chromosomes in anaphase or telophase.

Mouse in vivo tumorigenicity assay. Early (p9) and late passage (p37) MOSECs were cultured in serum-free medium for 6 before harvest then re-suspended in PBS at 5 x 10^6 cells per 200 μl, and injected intraperitoneally into 5-week-old female C57BL/6 mice purchased from National Rodent Laboratory Animal Center (Shanghai Branch). Control mice were injected with PBS. Animals were monitored weekly for the formation of ascites or tumors for up to 4 mo after injection. All mice were maintained according to the Institutional Animal Care and Use Committee of University of Science and Technology of China.

Histology and immunohistochemistry. Intestines were collected from mice, fixed in 4% paraformaldehyde and embedded in paraffin for histological analysis. For routine histology, tissue sections were stained with hematoxylin (BA-4097, Baso Diagnostics Inc.) according to standard protocols. For immunohistochemistry, following de-paraffinization, sections were re-hydrated in a series of graded ethanol/water solutions (100–95%-90–80%-70–50%) and PBS, boiled in 10 mM citric acid (pH 6.0) at 95–100°C for 10 min followed by incubation in 3% hydrogen peroxide for 10 min. Endogenous peroxidase was blocked by pre-incubation with 3% hydrogen peroxide for 10 min. A MOM mouse Ig blocking reagent (VECTOR M.O.M basic kit, BMK2202, Vector Laboratories, Inc.) was used to reduce nonspecific staining of mouse tissues by the mouse antibody. Then, the sections were incubated with a mouse anti-pan cytokeratin antibody (1:100) or a mouse anti-human PCNA monoclonal antibody (ZhongShan Goldenbridge Biotechnology CO.LTD, ZM-0213; 1:100) in a humidified chamber at 4°C overnight. After rising thoroughly with

TBS, the sections were exposed to a biotinylated anti-mouse IgG secondary antibody for 30 min (VECTOR M.O.M basic kit, BMK2202, Vector Laboratories, Inc.). The sections were rinsed again and exposed to peroxidase-conjugated streptavidin [UltraSensitive S-P (Mouse, Rabbit) Kit, Maxim.Bio, Inc.] for 30 min. Finally, each section was exposed to 3,3-diaminobenzidine solution (DAB kit, DAB0031, Maxim.Bio, Inc.) after they were rinsed with TBST. Immunostained sections were counterstained with hematoxylin, dehydrated through a series of alcohol (50–70%-80–90%-95–100%) and xylene, and covered with coverslips.

Statistical analysis. All statistical comparisons were performed using the 2 x 2 $\chi 2$ test. The p-values were as shown, and less than 0.05 were considered statistically significant.

Disclosure of Potential Conflicts of Interest

No potential conflicts of interest were disclosed.

Acknowledgments

We thank Katherine F. Roby from University of Kansas Medical Center, for kindly providing suggestion on primary cell culture. This work was supported by grants from National Natural Science Foundation of China (Grants 30671168, 30725013 and 30711120571) and Doctoral Fund of Ministry of Education of China.

Supplemental Materials

Supplemental materials may be found here:
www.landesbioscience.com/journals/cc/article/21196

References

1. Jemal A, Siegel R, Ward E, Hao Y, Xu J, Thun MJ. Cancer statistics, 2009. CA Cancer J Clin 2009; 59:225-49; PMID:19474385; http://dx.doi.org/10.3322/caac.20006.
2. Auersperg N, Wong AS, Choi KC, Kang SK, Leung PC. Ovarian surface epithelium: biology, endocrinology, and pathology. Endocr Rev 2001; 22:255-88; PMID:11294827; http://dx.doi.org/10.1210/er.22.2.255.
3. Riman T, Persson I, Nilsson S. Hormonal aspects of epithelial ovarian cancer: review of epidemiological evidence. Clin Endocrinol (Oxf) 1998; 49:695-707; PMID:10209555; http://dx.doi.org/10.1046/j.1365-2265.1998.00577.x.
4. Fathalla MF. Incessant ovulation--a factor in ovarian neoplasia? Lancet 1971; 2:163; PMID:4104488; http://dx.doi.org/10.1016/S0140-6736(71)92335-X.
5. Godwin AK, Testa JR, Handel LM, Liu Z, Vanderveer LA, Tracey PA, et al. Spontaneous transformation of rat ovarian surface epithelial cells: association with cytogenetic changes and implications of repeated ovulation in the etiology of ovarian cancer. J Natl Cancer Inst 1992; 84:592-601; PMID:1556770; http://dx.doi.org/10.1093/jnci/84.8.592.
6. Testa JR, Getts LA, Salazar H, Liu Z, Handel LM, Godwin AK, et al. Spontaneous transformation of rat ovarian surface epithelial cells results in well to poorly differentiated tumors with a parallel range of cytogenetic complexity. Cancer Res 1994; 54:2778-84; PMID:8168110.
7. Roby KF, Taylor CC, Sweetwood JP, Cheng Y, Pace JL, Tawfik O, et al. Development of a syngeneic mouse model for events related to ovarian cancer. Carcinogenesis 2000; 21:585-91; PMID:10753190; http://dx.doi.org/10.1093/carcin/21.4.585.
8. Roberts PC, Mottillo EP, Baxa AC, Heng HH, Doyon-Reale N, Gregoire L, et al. Sequential molecular and cellular events during neoplastic progression: a mouse syngeneic ovarian cancer model. Neoplasia 2005; 7:944-56; PMID:16242077; http://dx.doi.org/10.1593/neo.05358.
9. Holland AJ, Cleveland DW. Boveri revisited: chromosomal instability, aneuploidy and tumorigenesis. Nat Rev Mol Cell Biol 2009; 10:478-87; PMID:19546858; http://dx.doi.org/10.1038/nrm2718.
10. Weaver BA, Cleveland DW. Does aneuploidy cause cancer? Curr Opin Cell Biol 2006; 18:658-67; PMID:17046232; http://dx.doi.org/10.1016/j.ceb.2006.10.002.
11. Lassus H, Staff S, Leminen A, Isola J, Butzow R. Aurora-A overexpression and aneuploidy predict poor outcome in serous ovarian carcinoma. Gynecol Oncol 2011; 120:11-7; PMID:20937525; http://dx.doi.org/10.1016/j.ygyno.2010.09.003.
12. Kim YT, Zhao M, Kim SH, Lee CS, Kim JH, Kim JW. Prognostic significance of DNA quantification by flow cytometry in ovarian tumors. Int J Gynaecol Obstet 2005; 88:286-91; PMID:15733883; http://dx.doi.org/10.1016/j.ijgo.2004.12.010.
13. Ozalp S, Yalcin OT, Gulbas Z, Tanir HM, Minsin T. Effect of cellular DNA content on the prognosis of epithelial ovarian cancers. Gynecol Obstet Invest 2001; 52:93-7; PMID:11586035; http://dx.doi.org/10.1159/000052950.
14. Pothuri B, Leitao MM, Levine DA, Viale A, Olshen AB, Arroyo C, et al. Genetic analysis of the early natural history of epithelial ovarian carcinoma. PLoS One 2010; 5:e10358; PMID:20436685; http://dx.doi.org/10.1371/journal.pone.0010358.
15. Compton DA. Mechanisms of aneuploidy. Curr Opin Cell Biol 2011; 23:109-13; PMID:20810265; http://dx.doi.org/10.1016/j.ceb.2010.08.007.
16. Thompson SL, Bakhoum SF, Compton DA. Mechanisms of chromosomal instability. Curr Biol 2010; 20:R285-95; PMID:20334839; http://dx.doi.org/10.1016/j.cub.2010.01.034.
17. Boveri T, Boveri M. The origin of malignant tumors. Baltimore: The Williams & Wilkins Company, 1929.
18. Shackney SE, Smith CA, Miller BW, Burholt DR, Murtha K, Giles HR, et al. Model for the genetic evolution of human solid tumors. Cancer Res 1989; 49:3344-54; PMID:2720687.
19. Storchova Z, Pellman D. From polyploidy to aneuploidy, genome instability and cancer. Nat Rev Mol Cell Biol 2004; 5:45-54; PMID:14708009; http://dx.doi.org/10.1038/nrm1276.
20. Fujiwara T, Bandi M, Nitta M, Ivanova EV, Bronson RT, Pellman D. Cytokinesis failure generating tetraploids promotes tumorigenesis in p53-null cells. Nature 2005; 437:1043-7; PMID:16222300; http://dx.doi.org/10.1038/nature04217.
21. Shi Q, King RW. Chromosome nondisjunction yields tetraploid rather than aneuploid cells in human cell lines. Nature 2005; 437:1038-42; PMID:16222248; http://dx.doi.org/10.1038/nature03958.
22. Galipeau PC, Cowan DS, Sanchez CA, Barrett MT, Emond MJ, Levine DS, et al. 17p (p53) allelic losses, 4N (G2/tetraploid) populations, and progression to aneuploidy in Barrett's esophagus. Proc Natl Acad Sci USA 1996; 93:7081-4; PMID:8692948; http://dx.doi.org/10.1073/pnas.93.14.7081.
23. Olaharski AJ, Sotelo R, Solorza-Luna G, Gonsebatt ME, Guzman P, Mohar A, et al. Tetraploidy and chromosomal instability are early events during cervical carcinogenesis. Carcinogenesis 2006; 27:337-43; PMID:16123119; http://dx.doi.org/10.1093/carcin/bgi218.
24. Levine DS, Rabinovitch PS, Haggitt RC, Blount PL, Dean PJ, Rubin CE, et al. Distribution of aneuploid cell populations in ulcerative colitis with dysplasia or cancer. Gastroenterology 1991; 101:1198-210; PMID:1936790.
25. Yancik R. Ovarian cancer. Age contrasts in incidence, histology, disease stage at diagnosis, and mortality. Cancer 1993; 71(Suppl):517-23; PMID:8420671; http://dx.doi.org/10.1002/cncr.2820710205.
26. Chuaire-Noack L, Rondón-Lagos S, Ramírez-Corredor A, Ibáñez-Pinilla M, Ramírez-Clavijo S. Cytogenetic aberrations in primary cell cultures of the ovarian surface epithelium. Invest Clin 2010; 51:541-51; PMID:21361148.
27. Bayani J, Paderova J, Murphy J, Rosen B, Zielenska M, Squire JA. Distinct patterns of structural and numerical chromosomal instability characterize sporadic ovarian cancer. Neoplasia 2008; 10:1057-65; PMID:18813350.
28. Yoon BS, Kim YT, Kim S, Lee CS, Kim JW, Kim JH, et al. Prognostic value of nuclear DNA quantification and cyclin A expression in epithelial ovarian carcinoma. Eur J Obstet Gynecol Reprod Biol 2008; 136:110-5; PMID:17157431; http://dx.doi.org/10.1016/j.ejogrb.2006.10.008.
29. Kristensen GB, Kildal W, Abeler VM, Kaern J, Vergote I, Tropé CG, et al. Large-scale genomic instability predicts long-term outcome for women with invasive stage I ovarian cancer. Ann Oncol 2003; 14:1494-500; PMID:14504048; http://dx.doi.org/10.1093/annonc/mdg403.
30. Friedlander ML, Taylor IW, Russell P, Musgrove EA, Hedley DH, Tattersall MH. Ploidy as a prognostic factor in ovarian cancer. Int J Gynecol Pathol 1983; 2:55-63; PMID:6307906; http://dx.doi.org/10.1097/00004347-198301000-00005.
31. Tsao SW, Mok SC, Fey EG, Fletcher JA, Wan TS, Chew EC, et al. Characterization of human ovarian surface epithelial cells immortalized by human papilloma viral oncogenes (HPV-E6E7 ORFs). Exp Cell Res 1995; 218:499-507; PMID:7796885; http://dx.doi.org/10.1006/excr.1995.1184.
32. Davies BR, Steele IA, Edmondson RJ, Zwolinski SA, Saretzki G, von Zglinicki T, et al. Immortalisation of human ovarian surface epithelium with telomerase and temperature-sensitive SV40 large T antigen. Exp Cell Res 2003; 288:390-402; PMID:12915130; http://dx.doi.org/10.1016/S0014-4827(03)00218-0.
33. Caldwell CM, Green RA, Kaplan KB. APC mutations lead to cytokinetic failures in vitro and tetraploid genotypes in Min mice. J Cell Biol 2007; 178:1109-20; PMID:17893240; http://dx.doi.org/10.1083/jcb.200703186.
34. Rosario CO, Ko MA, Haffani YZ, Gladdy RA, Paderova J, Pollett A, et al. Plk4 is required for cytokinesis and maintenance of chromosomal stability. Proc Natl Acad Sci USA 2010; 107:6888-93; PMID:20348415; http://dx.doi.org/10.1073/pnas.0910941107.
35. Sagona AP, Stenmark H. Cytokinesis and cancer. FEBS Lett 2010; 584:2652-61; PMID:20371245; http://dx.doi.org/10.1016/j.febslet.2010.03.044.

36. Duelli DM, Padilla-Nash HM, Berman D, Murphy KM, Ried T, Lazebnik Y. A virus causes cancer by inducing massive chromosomal instability through cell fusion. Curr Biol 2007; 17:431-7; PMID:17320392; http://dx.doi.org/10.1016/j.cub.2007.01.049.
37. Mazumdar M, Lee JH, Sengupta K, Ried T, Rane S, Misteli T. Tumor formation via loss of a molecular motor protein. Curr Biol 2006; 16:1559-64; PMID:16890532; http://dx.doi.org/10.1016/j.cub.2006.06.029.
38. Ganem NJ, Storchova Z, Pellman D. Tetraploidy, aneuploidy and cancer. Curr Opin Genet Dev 2007; 17:157-62; PMID:17324569; http://dx.doi.org/10.1016/j.gde.2007.02.011.
39. Ganem NJ, Godinho SA, Pellman D. A mechanism linking extra centrosomes to chromosomal instability. Nature 2009; 460:278-82; PMID:19506557; http://dx.doi.org/10.1038/nature08136.
40. Silkworth WT, Nardi IK, Scholl LM, Cimini D. Multipolar spindle pole coalescence is a major source of kinetochore mis-attachment and chromosome mis-segregation in cancer cells. PLoS One 2009; 4:e6564; PMID:19668340; http://dx.doi.org/10.1371/journal.pone.0006564.
41. Cimini D, Howell B, Maddox P, Khodjakov A, Degrassi F, Salmon ED. Merotelic kinetochore orientation is a major mechanism of aneuploidy in mitotic mammalian tissue cells. J Cell Biol 2001; 153:517-27; PMID:11331303; http://dx.doi.org/10.1083/jcb.153.3.517.
42. Atkin NB. Modal DNA value and chromosome number in ovarian neoplasia. A clinical and histopathologic assessment. Cancer 1971; 27:1064-73; PMID:4325742; http://dx.doi.org/10.1002/1097-0142(197105)27:5<1064::AID-CNCR2820270510>3.0.CO;2-K.
43. Kusyk CJ, Seski JC, Medlin WV, Edwards CL. Progressive chromosome changes associated with different sites of one ovarian carcinoma. J Natl Cancer Inst 1981; 66:1021-5; PMID:6941036.
44. Wang X, Allen TD, May RJ, Lightfoot S, Houchen CW, Huycke MM. Enterococcus faecalis induces aneuploidy and tetraploidy in colonic epithelial cells through a bystander effect. Cancer Res 2008; 68:9909-17; PMID:19047172; http://dx.doi.org/10.1158/0008-5472.CAN-08-1551.
45. Umeda M, Murata-Kamiya N, Saito Y, Ohba Y, Takahashi M, Hatakeyama M. Helicobacter pylori CagA causes mitotic impairment and induces chromosomal instability. J Biol Chem 2009; 284:22166-72; PMID:19546211; http://dx.doi.org/10.1074/jbc.M109.035766.
46. Shi QH, Adler ID, Yu L, Zhang JX. Detection of numerical chromosomal aberrations in epididymal sperm of mice using three-color FISH with chromosome-specific DNA probes. Yi Chuan Xue Bao 1999; 26:458-67; PMID:10665221.
47. Shi Q, Adler ID, Zhang J, Zhang X, Shan X, Martin R. Incidence of mosaic cell lines in vivo and malsegregation of chromosome 21 in lymphocytes in vitro of trisomy 21 patients: detection by fluorescence in situ hybridization on binucleated lymphocytes. Hum Genet 2000; 106:29-35; PMID:10982178; http://dx.doi.org/10.1007/s004390051005.
48. Takahashi S, Qian J, Brown JA, Alcaraz A, Bostwick DG, Lieber MM, et al. Potential markers of prostate cancer aggressiveness detected by fluorescence in situ hybridization in needle biopsies. Cancer Res 1994; 54:3574-9; PMID:8012984.
49. Rao X, Zhang Y, Yi Q, Hou H, Xu B, Chu L, et al. Multiple origins of spontaneously arising micronuclei in HeLa cells: direct evidence from long-term live cell imaging. Mutat Res 2008; 646:41-9; PMID:18845170; http://dx.doi.org/10.1016/j.mrfmmm.2008.09.004.